Journal of Catalysis 259 (2008) 43–53

Contents lists available at ScienceDirect

Journal of Catalysis

www.elsevier.com/locate/jcat

Understanding the effect of postsynthesis ammonium treatment on the catalytic activity of Au/Ti-SBA-15 catalysts for the oxidation of propene

Elena Sacaliuc-Parvulescu [a], Heiner Friedrich [a], Regina Palkovits [a], Bert M. Weckhuysen [a,*], T. Alexander Nijhuis [b,*]

[a] Inorganic Chemistry and Catalysis, Department of Chemistry, Faculty of Science, Utrecht University, Sorbonnelaan 16, 3584 CA Utrecht, The Netherlands
[b] Eindhoven University of Technology, Chemical Reactor Engineering, P.O. Box 513, 5600 MB Eindhoven, The Netherlands

ARTICLE INFO

Article history:
Received 25 April 2008
Revised 20 July 2008
Accepted 21 July 2008
Available online 26 August 2008

Keywords:
Propene epoxidation
Gold
SBA-15
Postsynthesis treatment

ABSTRACT

Postsynthesis ammonium treatment induces a substantial increase in the catalytic activity of Au/Ti-SBA-15 catalysts for the direct vapor-phase epoxidation of propylene using hydrogen and oxygen. The PO formation rate of a calcined Au/Ti-SBA-15 catalyst prepared by this method increased from 4.3 $mg_{PO}\,h^{-1}\,g_{cat}^{-1}$ to 37.2 $mg_{PO}\,h^{-1}\,g_{cat}^{-1}$ at 200 °C compared with a catalyst prepared in an identical manner without this treatment. The catalysts were characterized by XRD, N_2-sorption, UV–vis–NIR DRS, ^{29}Si MAS NMR, FT-IR spectroscopy, and TEM to gain insight into the relationship between ammonia treatment and catalyst activity. ^{29}Si MAS NMR measurements proved that the ammonium nitrate solution caused hydrolysis of ≡Si–O–Si≡ or ≡Ti–O–Si≡ bonds, resulting in a Ti-SBA-15 surface with a greater amount of surface hydroxyl groups. FT-IR measurements indicated the presence of amine species that favor the homogeneous deposition of Au nanoparticles. This was confirmed by TEM measurements showing greater metal dispersion for NH_4NO_3-treated Au/Ti-SBA-15 materials.

1. Introduction

The gas-phase epoxidation of propene over various Au/Ti-substituted catalysts is an intriguing scientific topic, not only because of the great industrial importance of this process, but also because this reaction offers fundamental mechanistic insights into Au-based catalysis [1–4]. By volume, propene oxide is among the top 50 chemicals produced worldwide. It is an important building block for the production of surfactants, polyurethane, and solvents. The methods currently used for propene oxide synthesis (i.e., the chlorhydrin and hydroperoxide processes) have important disadvantages. The chlorhydrin process involves the production of chlorinated side products and calcium chloride waste, whereas the hydroperoxide process produces a stoichiometric amount of co-product [5]. The association of highly dispersed gold nanoparticles supported on titania (Au/TiO_2) has been found to highly selective epoxidise propene in the presence of hydrogen and oxygen under mild conditions (323 K), but only at very low conversion (~1%) [6]. Gold-based catalysts could become feasible for petrochemical industry if conversion (>10%) and hydrogen efficiency (>30%) could be increased together with stability with time-on-stream, while retaining high selectivity (>90%) [7,8]. This process is especially attractive because of its simplicity (single reaction/reactor) and thus could become a potential competitor for the new H_2O_2–PO process, which involves 3 different reaction steps.

In many publications, it has been suggested that catalyst performance depends on the nature of the support, site density and size, and the oxidation state of Au nanoparticles [6,9–14]. Proper choice of the support is critical. The approach to selecting the titanium support was inspired by liquid-phase epoxidation reactions, in which isolated titanium sites incorporated into different silica matrix are the active species [15,16]. When gold is deposited on TS-1, catalyst stability and PO yield improve when the reaction was performed at high temperature (473 K) [17,18]. It was found that the increase in epoxide yield also is dependent on the amount of isolated titanium species. The amount of titanium in the silica matrix must be carefully adjusted, because catalyst materials prepared from supports with an Si/Ti molar ratio >500 are able to generate propanal due to the increased acidic nature of the support, and an excessively high titanium concentration leads to unwanted side reactions and further oxidation [11]. Mesoporous silica supports, such as MCM-41, SBA-15, and MCM-48 with titanium dispersed as isolated species, have been found to be effective in the activity of propene epoxidation due to their pore size distribution, pore volume, and high surface area [19–22]. The activity of Au supported on Ti-MCM-48 exceeds that of Au supported on Ti-MCM-41, indicating that the three-dimensional branched pore structure is more suitable [21]. The drawback of MCM-41 and MCM-48 is that they are generally hydrothermally unstable, but materials like SBA-15 are preferable for catalysis applications because of their thicker pore walls (typically 3–9 nm) [23].

* Corresponding authors. Faxes: +31 30 251 1027, +31 40 244 6653.
E-mail addresses: b.m.weckhuysen@uu.nl (B.M. Weckhuysen), t.a.nijhuis@tue.nl (T.A. Nijhuis).

0021-9517/$ – see front matter
doi:10.1016/j.jcat.2008.07.013

The size and distribution of gold nanoparticles also are very important for their activity and selectivity in propene epoxidation with hydrogen and oxygen [11,14,18,24,25]. The synthesis route, like the way of reducing the gold, the pH of the solution, the source of gold and the physical–chemical properties of the support, are greatly influenced by the size and distribution of the gold nanoparticles. But only a portion of gold deposited on the surface of the catalysts creates active Au–Ti epoxidation centers; thus, it is very important to maximize the number of deposited gold nanoparticles on the support and eventually their proximity to the Ti species [11,14,26]. This can be influenced both by the method of gold deposition and by modification of the support properties. Each support has a specific capacity for gold capture during deposition–precipitation. To maximize the adsorption capacity, it is very important to choose the proper type of the support or to perform further pretreatments to obtain narrow well-dispersed gold nanoparticles. Delgass et al. [14] showed that an NH_4NO_3 treatment of TS-1 material can enhance gold capture during the deposition–precipitation procedure.

In this work, we investigate the influence of postsynthesis ammonium treatment of Ti-SBA-15 support on the morphology of gold nanoparticles and their catalytic performance in the propene epoxidation. By using various characterization methods, it is possible to put forward plausible explanations for the observed difference in catalytic performances.

2. Experimental

2.1. Catalyst preparation

Pure mesoporous silica SBA-15 material was hydrothermally synthesized according to the procedure described by Zhao [27]. The reagent used were poly(ethylene glycol)-*block*-poly(propylene glycol)-*block*-poly(ethylene glycol) (PEG–PPG–PEG) (average molecular weight 5800, Aldrich), tetraethylortosilicate (Aldrich, 98%), HCl (Merck, 37%), and distilled water. The gel solution was prepared by dispersing 8 g of PEG–PPG–PEG in 60 g of distilled water, followed by 15 min of vigorous stirring at 40 °C. The resultant solution was mixed with 48 g HCl and 190 g H_2O and stirred for another 17 h. Finally, 21.2 g tetraethylortosilicate solution was added dropwise in the gel mixture at 40 °C with stirring for 9 h before being placed in a Teflon autoclave at 100 °C for 12 h. After the completion of synthesis, the product was filtered, washed with distilled water, and air-dried overnight at 60 °C. The solid was calcined at 550 °C for 6 h.

The Ti-SBA-15 grafted support, designated Ti-G, with a Si/Ti molar ratio of 40, was synthesized using titanium isopropoxide (Across, 98%) as a titanium source [28]. Titanium grafting was performed inside a glove box in nitrogen environment. Titanium(IV) isopropoxide was dispersed in 2 g of dry isopropyl alcohol (99.7%, Merck) and mixed with 1 g of SBA-15 at ambient temperature. The solid was dried at ambient temperature under flowing nitrogen. Finally, the titanium-grafted material was calcined at 400 °C for 4 h.

The postsynthesis ammonium treatment was carried using NH_4NO_3 (1 M) solution [14]. Ammonium-treated Ti-SBA-15 supports were prepared by suspending 1 g of calcined Ti-SBA-15 material in 60 g of NH_4NO_3 solution. The solution was heated at 80 °C under continuous stirring from 6 h to 30 h. The product thus obtained was washed with 80 g of deionized water and dried at 60 °C overnight. The resulting samples were labeled Ti-N-n, with n representing the ammonium treatment time. The ammonium-treated Ti-SBA-15 supports were not calcined before the Au deposition. A postsynthesis water treatment was also carried out, following the same procedure as in ammonium treatment. The water-treated Ti-SBA-15 support was designated Ti-H-30.

Au catalysts, designated Au/Ti-N-n and Au/Ti-H-30h, were prepared by the deposition-precipitation method [14] using aqueous $HAuCl_4$ solution corresponding to 1 wt% Au and Na_2CO_3 (1 M) as precipitant. In this method, $HAuCl_4$ solution was dissolved in 50 ml of deionised water, followed by the dispersion of 1 g of Ti-SBA-15 support. The solution mixture was stirred for 15 min before the pH was adjusted to 9 with 1 M Na_2CO_3. The mixture was stirred at room temperature for 4 h, with the pH maintained at 9. The catalysts were washed with distilled water, dried in air overnight at 60 °C, and calcined at 400 °C for 4 h. To understand the effect of the ammonium treatment, an Au/Ti-G catalyst was prepared as a reference.

An Au**N**-Ti-n catalyst was synthesized by changing the order of Au and Ti incorporation. In this preparation procedure, calcined SBA-15 material was treated with ammonium before Au deposition, after which titanium grafting was performed on the calcined 1% AuN material.

2.2. Catalyst characterization

The degree of crystallinity and morphology of the obtained Au–Ti-SBA-15 materials was characterized using transmission electron microscopy (TEM) and X-ray diffraction (XRD). The latter was performed using a Bruker-AXS D8 Advance powder X-ray diffractometer, equipped with automatic divergence slit, Våntec-1 detector, and cobalt $K\alpha_{1,2}$ ($\lambda = 1.79026$ Å) source.

TEM images were acquired in bright-field mode using a Tecnai F20 electron microscope (FEI Company). The microscope, operated at 200 keV, was equipped with a field emission gun, a twin objective lens, and a $1k \times 1k$ Gatan Slow Scan CCD camera. TEM sample preparation proceeded as follows. A small portion of dry powder (~15 mg) was placed in a 16-mm mold/die commonly used for pelletization. The powder was then pressed to a peak weight of approximately 12 tons (460 MPa), after which the pressure was immediately released. The resulting pellet was ground up in a mortar, and a small portion of the very fine powder was dispersed in etanol by ultrasonication for 30 s. Finally, a few droplets of the suspension were placed on a Quantifoil R2/1 lacey carbon support film and dried under a lamp. The additional step of compressing the SBA-15 powder before conventional TEM sample preparation was found to be advantageous for imaging of the examined material. As shown in earlier work, imaging of small metal (oxide) particles in the pores of SBA-15 can be carried out by electron tomography [29–31]. However, for conventional TEM, imaging of small metal (oxide) particles through large or thick SBA-15 structures is difficult. In this case, very thin support structures are advantageous. During pressing of the material, the SBA-15 particles, roughly 2000 × 500 × 500 nm in size, fracture, leaving much smaller and thinner pieces intact. Very small Au particles are found in the pores of theses thin pieces. Parts of the SBA-15 structure collapse, resulting in disordered amorphous silica. Comparison of pressed and unpressed material ensured that pressing did not affect the gold particle.

The particle size distribution was estimated by measuring the diameter of more than 100 particles in each sample using Analysis software. The corresponding volume and surface area weighted distributions were calculated directly from the particle diameters, assuming a spherical particle shape. The specific surface area and pore volume were determined by N_2 sorption measurements using a Micromeritics ASAP 2400 instrument. Surface areas were calculated using the BET model, with micropores and macropores described by the Horvath–Kawazoe and BJH models, respectively.

UV–vis–NIR diffuse reflectance spectroscopy (DRS) measurements were carried out at room temperature on a Varian Cary 500 instrument in the range of 200–2200 nm. This set-up was equipped with a diffuse reflectance accessory, which was set to

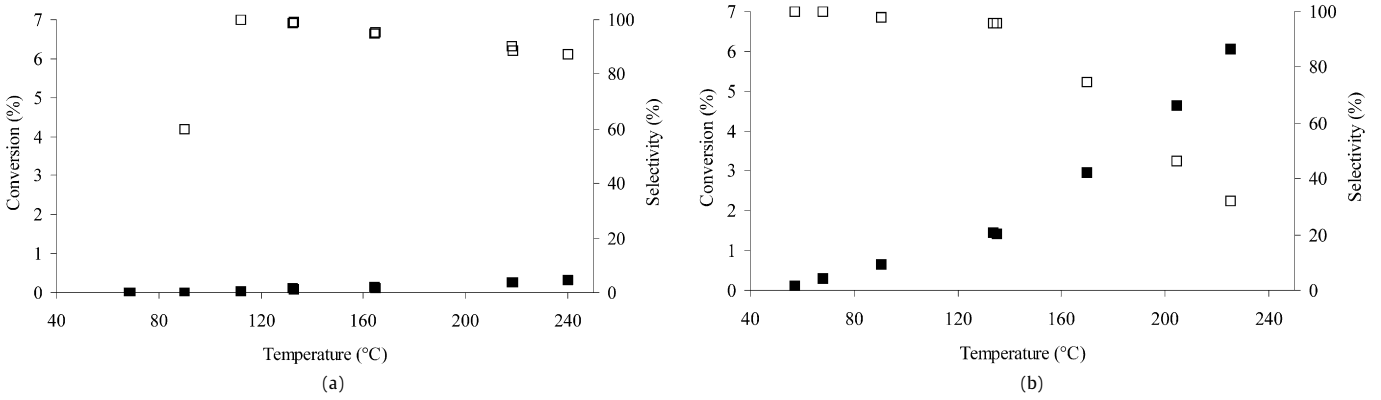

Fig. 1. Catalytic performance of (a) Au-Ti-G and (b) Au/Ti-N-30 (conversion (■) and selectivity (□)).

Table 1
Overview of the catalytic performances of the different Au/Ti-SBA-15 catalyst materials under investigation[a]

Catalyst	Temperature (°C)	C (%) C_3H_6	Selectivity, S (%)					H_2 eff (%)
			PO	CO_2	Propanol	Propane	Other oxygenates	
Au/Ti-N-6h	90	0.4	99.4	0	0.6	0	0	4.59
	135	0.8	97.7	0	1.1	0	1.2	3.27
	170	1.6	89.3	7.67	1.47	0	1.56	2.67
	200	2.7	65	31.9	1.94	0	1.16	1.54
Au/Ti-**N**-15h	90	0.5	97.4	0	1.87	0	0.73	3.83
	135	0.9	92.7	0	1.7	3.67	1.93	2.81
	170	1.9	82.9	11.14	2.42	0.69	2.85	2.26
	200	3.2	58.4	38.97	0	0	2.63	1.4
Au/Ti-N-30h	90	0.7	98	0	1.29	0	0.71	5.46
	135	1.4	95.7	1	1.32	0	1.98	3.63
	170	2.8	74.6	21.2	1.73	0	2.47	2.22
	200	4.6	46.4	50.28	2	0	1.32	1.38
Au**N**-Ti-15h	90	0.4	98.7	0	1.3	0	0	12.44
	135	0.7	96.5	0	3.5	0	0	8.47
	170	0.8	89	0.06	10.94	0	0	4.5
	200	1.9	39.7	33.65	26.65	0	0	0.92
Au-Ti-G	90	0	0	0	0	0	0	0
	135	0.08	98.9	0	0	0	1.1	14.13
	170	0.13	95.2	0	2.8	0	2	11.86
	200	0.2	90.1	0	5.18	0	4.72	4.55

[a] C—conversion, S—selectivity.

collect diffuse reflected light only. A baseline correction was performed using a white Halon standard. ^{29}Si MAS NMR measurements were carried out with a Bruker Avance 500WB spectrometer at a spinning rate of 10 kHz using $\pi/4$ pulses of 2.2 μs and a repetition delay of 30 s. FT-IR spectra were recorded on a Perkin-Elmer Spectrum One instrument on self-supported catalyst wafers placed in an IR transmission cell equipped with CaF_2 windows. For each sample, an IR spectrum was recorded before and after drying in helium at 300 °C.

2.3. Catalyst testing

A flow reactor was used to evaluate the catalytic performance of the different catalysts prepared. The experiments were carried out typically with 0.4 g of catalyst material and a flow of 50 Nml min^{-1}. The gas mixture consisted of 10% oxygen, 10% hydrogen, and 10% propene in He. The analysis of the gas leaving the reactor was carried out using an Interscience Compact GC system, equipped with a Molsieve 5A and a Porabond Q column, each with a thermal conductivity detector (TCD). Gas samples were analyzed every 3 min. The experiments were carried out in cycles: 5 h at reaction temperature with the reactant mixture, followed by a regeneration cycle. In regeneration, 10% oxygen in helium was used, and the catalyst was heated at 300 °C and maintained at that temperature 1 h, then cooled to the next reaction temperature in the cycle. The performance was typically tested at 10–15 different temperatures (including duplicates to determine for each catalyst the deactivation pattern).

3. Results

Fig. 1 shows the catalytic activities of different Au/Ti-SBA-15 samples in the propene epoxidation reaction with O_2 and H_2. The untreated Au/Ti-G catalyst showed relatively low activity under the reaction conditions. This activity is typical for unmodified Au/TS-1 catalyst under these conditions. But the Au/Ti-N-30h catalyst with Au supported on NH_4NO_3-pretreated Ti-SBA-15 support showed substantial activity for propene oxide formation. NH_4NO_3 treatment clearly exerted a pronounced effect on the catalytic performance of the Au/Ti-N-30 catalyst. As the reaction temperature was increased, the selectivity to propene oxide decreased, corresponding to an increase in total oxidation products.

The conversion, selectivity, hydrogen efficiency, and product distribution of the different Au/Ti-SBA-15 catalysts studied are summarized in Table 1. All catalysts exhibited higher conversion levels with increasing reaction temperature, but at the expense of the selectivity toward propene oxide due to an increase in total ox-

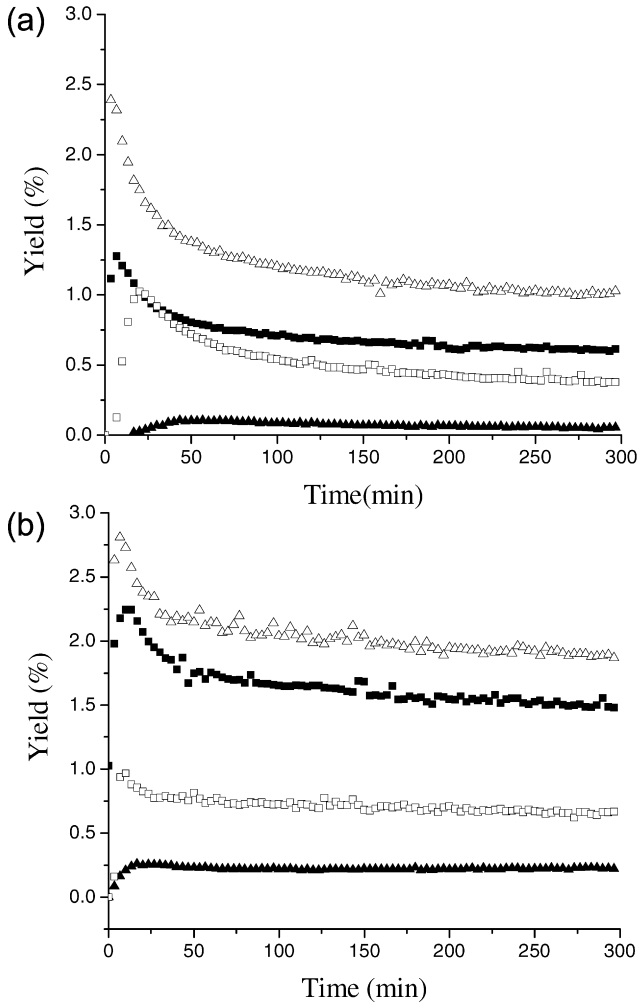

Fig. 2. Catalytic performance of Au-based catalyst materials tested at two different temperatures (a) 130 °C and (b) 200 °C. The catalyst materials are: (▲) Au-Ti-G, (□) AuN–Ti-15h, (■) Au/Ti-N-6h and (△) Au/Ti-N-30h. 0.4 g catalyst, 50 Nml min^{-1} gas federate (10% H_2, O_2, propene), total pressure 1100 mbar.

idation to CO_2. The water-treated Au/Ti-H-30h catalyst was inactive in propene epoxidation reaction, with propane the main product.

Another important finding is that the catalytic activity of the Au/Ti-N-n materials was enhanced when the NH_4NO_3 treatment of Ti/SBA-15 support was increased from 6 h to 30 h. Fig. 2 shows the yields of propene oxide over different Au/Ti-SBA-15 catalysts as a function of time on stream. The propene oxide yields were lower for the Au–Ti-G and AuN–Ti-15h catalysts than for the Au/Ti-N-30h catalyst. Small losses in the activity of Au/Ti-SBA-15 catalysts at 200 °C during 5 h time on stream were seen, although catalytic activity could be restored almost completely after an activation procedure at 300 °C. Comparing the activities of Au/Ti-SBA-15 catalysts for which the order of Au and Ti incorporation differed shows that the Au/Ti-N-15h material had greater catalytic activity than the AuN–Ti-15h material. Propene oxide production was measured after 3–5 h of steady-state activity at 200 °C. The Au-Ti-G catalyst had a rate of 4.3 $mg_{PO}\,h^{-1}\,g_{cat}^{-1}$, whereas the NH_4NO_3 treated Au/Ti-N-30h catalyst had a rate of 37.2 $mg_{PO}\,h^{-1}\,g_{cat}^{-1}$. Delgass et al. [14] previously reported this substantially increased catalytic activity of NH_4NO_3-treated catalyst materials for Au/TS-1 materials. This group explained the observed differences in catalytic performances in terms of increasing active site density. The reason for the increased number of active sites due to NH_4NO_3 treatment remains unclear, however; Delgass et al. suggested that the formation of an Au-amine complex near Ti sites could be responsible

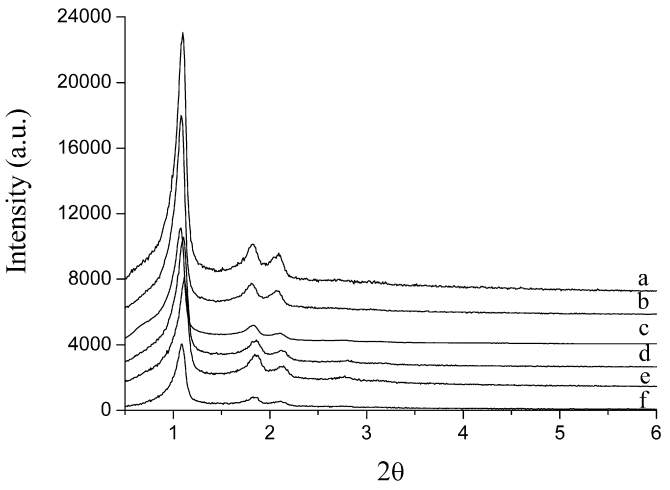

Fig. 3. Small angle XRD patterns of: (a) SBA-15, (b) Ti-G, (c) Au**N**–Ti-15h, (d) Au/Ti-N-6h, (e) Au/Ti-N-15h, and (f) Au/Ti-N-30h.

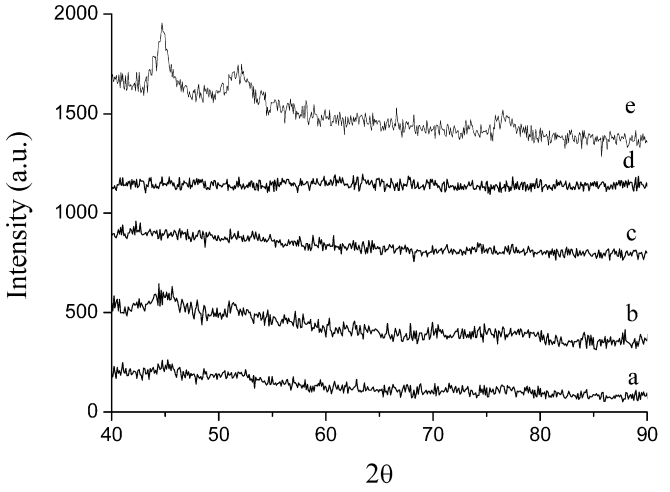

Fig. 4. Wide angle XRD patterns of: (a) Au/Ti-N-6h, (b) Au/Ti-N-15h, (c) Au/Ti-N-30h, (d) Au-Ti-G, and (e) Au**N**-Ti-15h.

for boosting the catalytic activity of NH_4NO_3-treated Au/TS-1 catalysts. To gain more insight into this boosting effect, we thoroughly characterized the different Au/Ti-SBA-15 catalyst materials under investigation through various techniques.

3.1. X-ray diffraction

The powder XRD patterns of the calcined samples are shown in Figs. 3 and 4. In the small-angle region of the XRD patterns (Fig. 3), all of the samples exhibit three well-resolved diffraction peaks that can be indexed to (100), (110), and (200) reflections of the *p6mm* hexagonal space group, which matches with the topology of SBA-15 structure [27]. After incorporation of Ti, the SBA-15 structure was preserved, as shown by the presence of intense reflection peaks of the Ti-SBA-15 sample. But the intensities of the peaks decreased in the case of ammonium-treated Au/Ti-SBA-15 samples, with this tendency even more pronounced with increasing ammonium treatment time. These results may indicate that the incorporation of Au and the increase in ammonium treatment time from 6 h to 30 h decreased the long-range order of the SBA-15 structure. XRD data from the high-angle region of the Au/Ti-SBA-15 samples are shown in Fig. 4. The absence of the gold peaks for the ammonium-treated Au/Ti-SBA-15 samples indicates that gold nanoparticles were highly dispersed

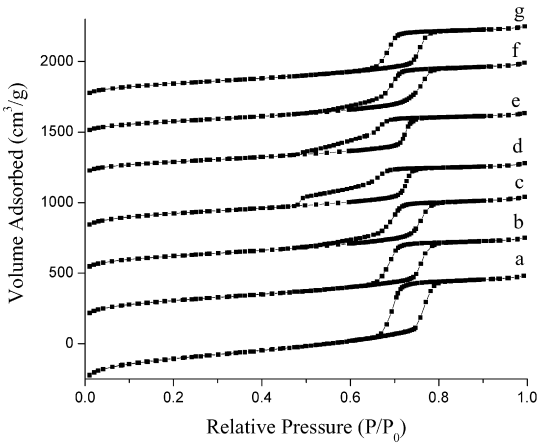

Fig. 5. N_2 adsorption–desorption isotherms of: (a) SBA-15, (b) Ti-G, (c) Ti-N-30h calcined, (d) Ti-H-30h, (e) Au/Ti-H-30h, (f) Au/Ti-N-30h, and (g) Au-Ti-G.

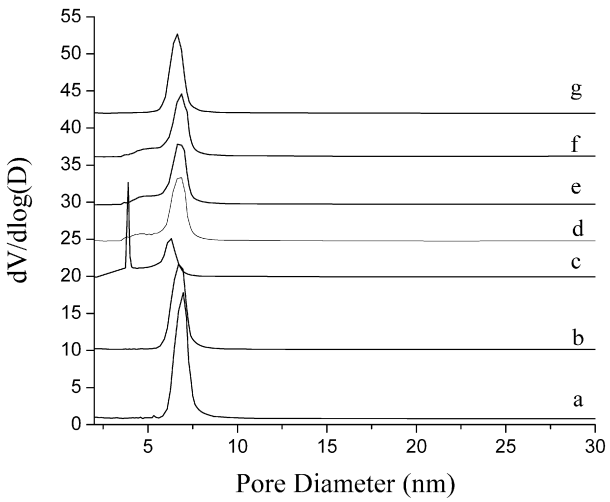

Fig. 6. Pore size distributions derived from desorption branches of N_2-sorption isotherms of: (a) SBA-15, (b) Ti-G, (c) Ti-H-30h, (d) Ti-N-30h calcined, (e) Au/Ti-N-6h, (f) Au/Ti-N-30h, and (g) Au-Ti-G.

through the silica matrix and that the average particles size was too small to be detected by XRD. Interestingly, in the Au**N**-Ti-15h sample, broad reflections of Au were seen, due to the formation of larger Au nanoparticles inside the channels of the SBA-15 support.

3.2. N_2 sorption measurements

Nitrogen adsorption–desorption isotherms of all synthesized samples are displayed in Fig. 5. The calcined samples exhibit type IV isotherms with H1-type hysteresis, typical of mesoporous materials with one-dimensional cylindrical channels [32]. The sharp inflection between the relative pressure P/Po 0.66 and 0.8 observed in the isotherm of SBA-15 correspond to the capillary condensation within uniform mesopores. The sharpening of this step reflects the uniform pore size distribution in the material. The introduction of Ti induced a decrease in the BET surface area of SBA-15 material from 972 $m^2 g^{-1}$ to 738 $m^2 g^{-1}$ and a decrease in pore volume from 1.3 $m^3 g^{-1}$ to 1 $m^3 g^{-1}$ (Table 2). The BET surface area and pore volume of Ti-SBA-15 also were modified after the 6-h ammonium treatment and changed slightly when this treatment was prolonged to 30 h. The decreased specific surface area of the ammonium-treated Ti-SBA-15 supports likely is caused by the modification of the Ti-SBA-15 structure.

Fig. 6 shows the BJH pore size distribution of the samples. The Ti-SBA-15 supports exhibited a bimodal structure after the water and ammonium treatment, both of which can cause hydrolysis of ≡Si–O–Si≡ or ≡Ti–O–Si≡ bonds, which may be associated with the formation of smaller pores in the structure. The introduction of Au inside the SBA-15 channels also induced a decrease in the pore volume and BET surface area of the Ti-SBA-15 material, demonstrated that some pore blocking occurred during Au incorporation [33]. Interestingly, the decrease in the pore volume was more pronounced in the AuN–Ti-15h sample than in the Au/Ti-N-15h sample. This suggests that the order of Au and Ti incorporation also has an influence on the textural properties of the resulting material, likely due to the presence of larger Au nanoparticles in the SBA-15 channels, as was seen in the XRD spectrum (Fig. 2).

3.3. UV–vis–NIR diffuse reflectance spectroscopy

DRS in the UV–vis–NIR region can distinguish the presence of framework and extra-framework titanium species in a silica matrix [34,35]. Representative UV–vis–NIR DRS spectra of the samples are shown in Fig. 7. In all DRS spectra of the titanium-containing SBA-15 samples, an intense band centered at ca. 220 nm can be observed, along with a shoulder at 260–270 nm. The band at 220 nm is due to the charge-transfer process of isolated framework titanium in tetrahedral coordination [34]. The shoulder at 270 nm has been attributed to the presence of Ti in fivefold and sixfold coordination, generated through the hydration of tetrahedrally coordinated sites [36]. Note that the intensity of this shoulder is much lower for the as-synthesized Ti-N-n supports than for the calcined Ti-N-n supports. These results suggest that the Ti environment for as-synthesized ammonium-treated Ti-SBA-15 supports differed than after calcination. Moreover, the intensity of the shoulder at 270 nm decreased after NH_4NO_3 treatment, as seen by comparing the Ti-G support with the calcined Ti-N-6h support (Fig. 7, spectra a and e). The UV–vis–NIR DRS spectra cannot be used to estimate the quantity of titanium in the sample, but the variation in the intensity may reflect changes in the amount and type of species of Ti

Table 2
Summary of the characterization results of the different SBA-15, Ti-SBA-15 and Au/Ti-SBA-15, samples under study

Catalyst	Si/Ti final molar ratio	Au loading (wt%)	BET surface area ($m^2 g^{-1}$)	Micropore vol. ($cm^3 g^{-1}$)	t-Plot area ($m^2 g^{-1}$)	Pore volume BJH ($cm^3 g^{-1}$)	Pore size BJH desorption (nm)
SBA-15	–	–	970	0.07	810	1.3	6.9
Ti-G	43.0	–	740	0.05	615	1	6.8
Ti-**N**-6h (calcined)	43.5	–	640	0.04	550	0.92	4.6; 6.9
Ti-**N**-30h (calcined)	49.4	–	615	0.03	525	0.9	4.6; 6.9
Ti-H-30h	48.3	–	648	0.06	512	0.86	3.8; 6.3
Au/Ti-H-30h	–	0.05	483	0.01	447	0.74	3.8; 6.3
Au/Ti-**N**-6h	–	1	480	0.007	460	0.83	4.6; 6.9
Au/Ti-**N**-15h	–	1	510	0.009	475	0.87	4.6; 6.9
Au/Ti-**N**-30h	–	1	490	0.007	460	0.83	4.6; 6.9
Au–Ti-G	–	0.1	510	0.006	490	0.83	6.6
Au**N**–Ti-15h	–	1	430	0.009	440	0.82	6.8

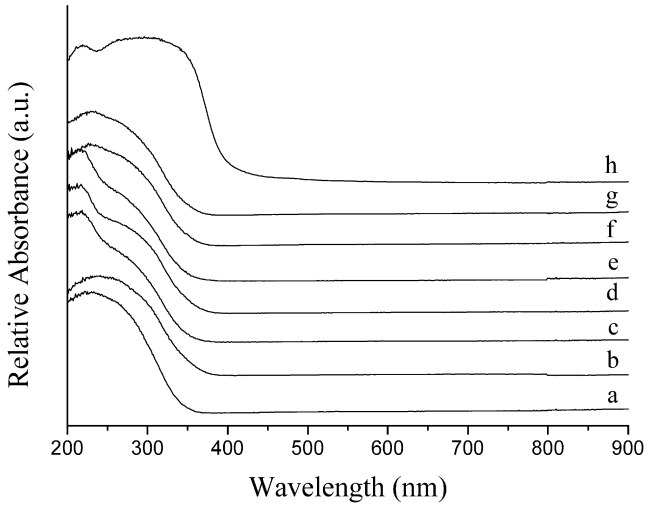

Fig. 7. UV–vis–NIR DR spectra of Ti-SBA-15 supports: (a) Ti-G, (b) Ti-H-30h (c) Ti-N-6h, (d) Ti-N-15h, (e) Ti-N-30h, (f) Ti-N-6h calcined, (g) Ti-N-30h calcined, and (h) TiO_2 anatase.

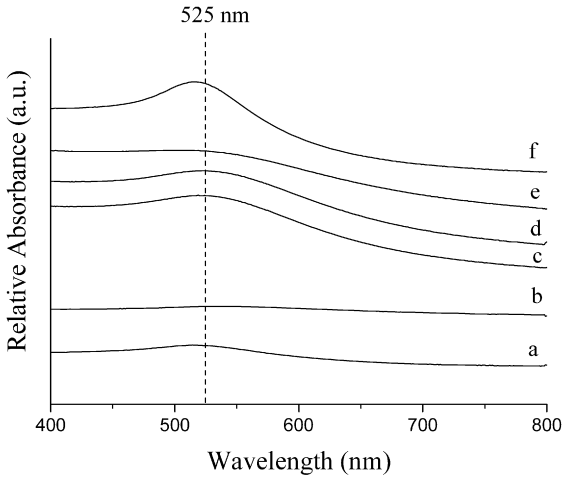

Fig. 8. UV–vis–NIR DR spectra of Au/Ti-SBA-15 samples of: (a) Au-Ti-G, (b) Au/Ti-H-30h, (c) Au/Ti-N-6h, (d) Au /Ti-N-15h, (e) Au/Ti-N-30h, and (f) Au**N**-Ti-15h.

in Ti-SBA-15 after the ammonium treatment. These results confirm that during NH_4NO_3 treatment, some extra-framework titanium was removed from the surface of SBA-15, in good agreement with the ICP-AES results. Note that the spectrum of the water-treated Ti-H-30h sample (Fig. 7b) is similar to that of the Ti-G support (Fig. 7a). The absence of a band at 330–340 nm indicates that no bulk titania was formed during synthesis [36]. The presence of a UV–vis absorption band at around 520 nm results from the plasmon resonance of nanosized metallic gold particles present in the Au/Ti-SBA-15 samples (Fig. 8) [37]. The intensity of this band was greater for the AuN/Ti-15h sample than for the Au/Ti-N-n samples, confirming the presence of smaller Au particles in the Au/Ti-N-n samples, as also demonstrated in the XRD pattern analysis.

3.4. ^{29}Si MAS NMR spectroscopy

^{29}Si MAS NMR spectroscopy can provide information about the nature and amount of silanol groups present in the Ti-SBA-15 mesostructure [38,39]. The ^{29}Si NMR spectra for the calcined SBA-15, Ti-SBA-15, Au-Ti-SBA-15, and as-synthesized Ti-N-n supports are shown in Fig. 9. For the calcined SBA-15 and Ti-SBA-15 materials (Fig. 9, spectra a and b), the ^{29}Si NMR spectra have an intense resonance peak at about −107 ppm, associated with silicon

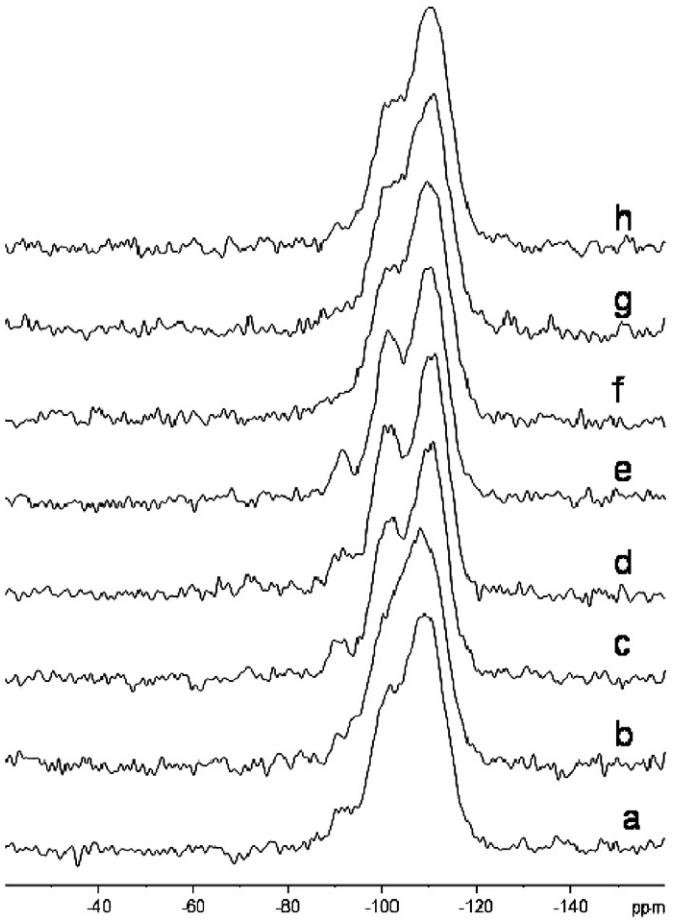

Fig. 9. ^{29}Si MAS NMR spectra of: (a) SBA-15 calcined, (b) Ti-G calcined, (c) Ti-N-6h as synthesized, (d) Ti-N-15h as synthesized, (e) Ti-N-30h as synthesized, (f) Au/Ti-N-30h calcined, (g) Au-Ti-G calcined, and (h) Au**N**-Ti-15h calcined.

linked via siloxane bridges to four other silicon atoms, $(\equiv SiO)_4Si$, designated Q^4. The two downfield resonance peaks at −97 and −89 ppm are attributed to silicon in single silanols, $(\equiv SiO)_3SiOH$, designated Q^3, and geminal silanols, $(\equiv SiO)_2Si(OH)_2$, designated Q^2 [40], respectively. The spectra of Ti-SBA-15 before (Fig. 9b) and after treatment with NH_4NO_3 (Fig. 9, spectra c, d, and e) are considerably different. A significant increase in signal intensity of the peaks at −97 and −89 ppm occurred after the NH_4NO_3 treatment (Fig. 9, spectra c, d, and e); however, the duration of this treatment did not seem to be reflected in comparable spectra after 6, 15, or 30 h of treatment time. ^{29}Si NMR spectra of Ti-SBA-15 supports before and after water treatment are shown in Fig. 10. Again, an increase in the intensity of Q^2 and Q^3 species can be seen, caused in this case by the water treatment (Fig. 10b), which is similar to the effect of the NH_4NO_3 treatment.

The increased intensity of Q^2 and Q^3 species on pretreatment of Ti-SBA-15 with 1 M solution of NH_4NO_3 or with water can be associated with a partial hydrolysis of some of ≡Si–O–Si≡ or ≡Ti–O–Si≡ bonds according to Scheme 1, resulting in increased density of surface hydroxyl groups. The possibility that these two resonance peaks also may contain contributions from Si(3Si, 1Ti) sites and from Si(2Si, 1Ti, 1H) sites cannot be excluded, however.

^{29}Si MAS NMR spectra of the Au/Ti-SBA-15 samples (Fig. 9, spectra f, g, and h) after gold deposition and calcination again exhibited reduced intensity of the Q^2 and Q^3 signals, which can be assigned to a decrease in surface hydroxyl groups due to condensation during the calcination procedure.

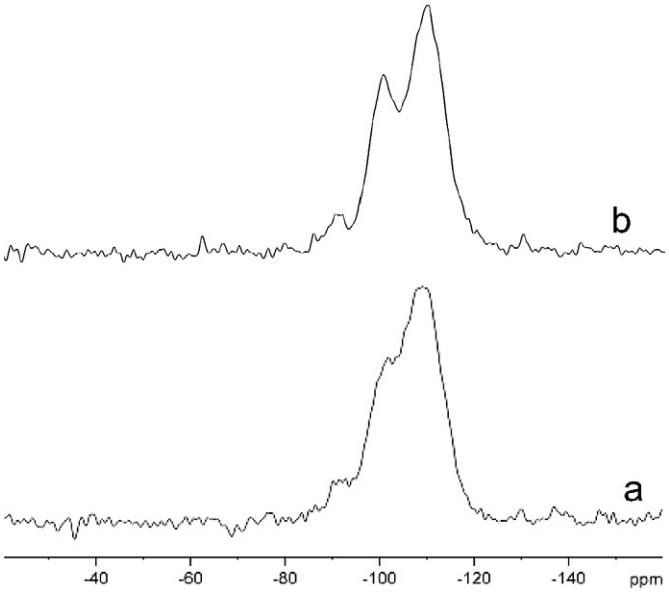

Fig. 10. ^{29}Si MAS NMR spectra of: (a) Ti-G calcined and (b) Ti-H-30 as synthesized.

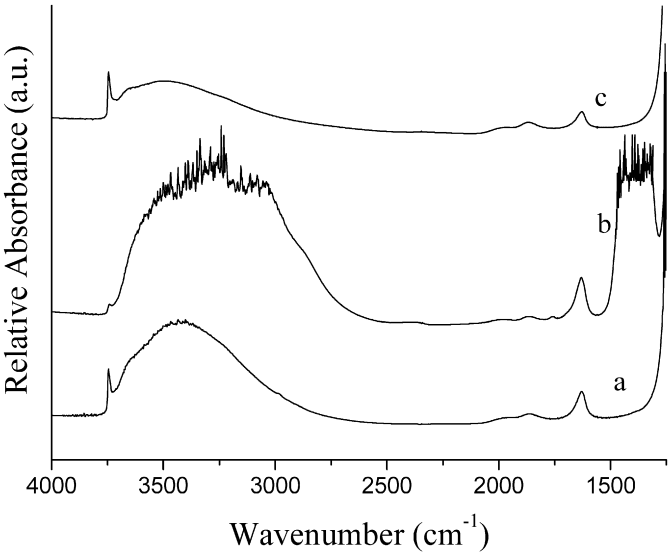

Fig. 11. IR spectra of: (a) Ti-G, (b) Ti-N-30h, (c) Au/Ti-N-30h recorded at room temperature.

3.5. FT-IR spectroscopy

Fig. 11 shows the IR spectra of Ti-G (a), Ti-N-30h (b), and Au/Ti-N-30h (c) before the thermal treatment. A narrow band at 3750 cm^{-1} and a broad absorption band in the 3700–3300 cm^{-1} range can be seen for all samples. The band at 3750 cm^{-1} is assigned to the OH stretching vibration of isolated silanol or geminal silanol groups located at the surface of the inner walls of the SBA-15 channels [40]. The absorption band in the 1700–1600 cm^{-1} region can be attributed to the water deformation vibration. The presence of NH_4NO_3 after postsynthesis treatment of the Ti-N-30h sample (Fig. 11b) is confirmed by the presence of two broad absorption bands at 1500–1250 cm^{-1} and 3600–3300 cm^{-1}, which can be assigned to the NH_4^+ bending and stretching vibrations. After the thermal treatment at 300 °C in helium (Fig. 12b), decomposition of NH_4NO_3 occurred, and the spectra of all samples became similar. The band at 3750 cm^{-1} became sharper and more intense, whereas the bands at 3700–3300 cm^{-1} and 1700–1600 cm^{-1} decreased in intensity during thermal treatment because of water and NH_4NO_3 removal.

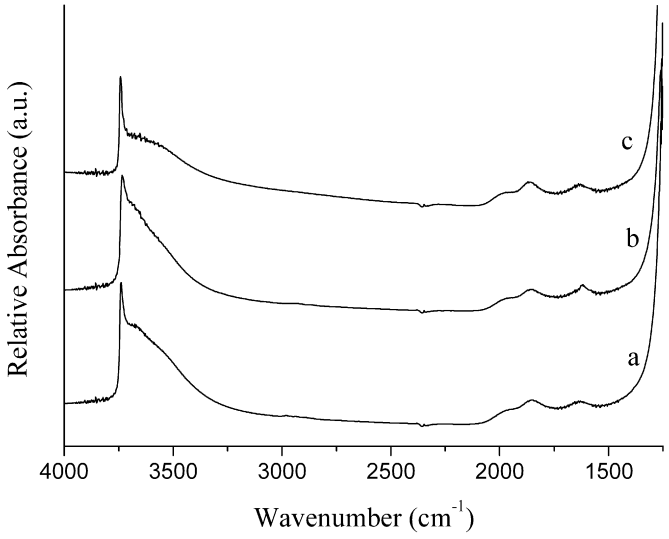

Fig. 12. IR spectra of: (a) Ti-G, (b) Ti-N-30h, (c) Au/Ti-N-30h recorded after thermal treatment at 300 °C.

$$\text{Ti-O-Si} \xrightarrow[\text{pH=5}]{NH_4^+NO_3^- / H_2O} \text{Si-OH + Ti-OH}$$

Scheme 1. NH_4NO_3 treatment of Ti-SBA-15 material.

3.6. Transmission electron microscopy

To gain more insight into the effect of the postsynthesis NH_4NO_3 treatment and water treatment, the Au/Ti-SBA-15 materials were analyzed by TEM. Fig. 13 presents TEM micrographs of Au/Ti-SBA-15 samples with (Au/Ti-N-30h) and without (Au/Ti-G) NH_4NO_3 treatment of the support before the gold deposition. The corresponding number-, surface-, and volume-weighted particle size distributions [41] are given in Fig. 14. The TEM image of the Au/Ti-G material (Fig. 13a) shows that very few Au particles were deposited on the support, in good agreement with ICP-AES results. Furthermore, Au particles were not well dispersed in the channels of Ti-SBA-15; some of them, mainly large particles, seemed to be formed on the outer surface of the support. The Au particles in this sample had an average particle diameter of 5 nm (number-weighted), 11 nm (surface-weighted), and 15 nm (volume-weighted). It was difficult to determine the exact location of the gold nanoparticles from the TEM micrographs of the water treated Au/Ti-H-30 sample (not shown), however, presumably because of the very low gold loading deposited on the water-treated Ti-SBA-15 supports. The TEM image of the Au/Ti-N-30h sample (Fig. 13b) clearly shows the presence only of small gold nanoparticles. In addition, particles with a mean diameter of 2–3 nm (number weighted), 4 nm (surface weighted), and 5 nm (volume weighted), were dispersed homogeneously in the Ti/SBA-15 mesopores. The need for titanium in the SBA-15 structure to ensure good Au dispersion/adsorption is clearly demonstrated by the TEM micrograph of the AuN/Ti-15h sample (Fig. 13c), for which Au was first deposited on an NH_4NO_3 pretreated SBA-15 and Ti was then grafted. In this case, larger Au nanoparticles were formed, comparable with those in the Au/Ti-N-30h sample in which the Ti-SBA-15 support was pretreated before Au deposition. The average diameter of Au nanoparticles for AuN/Ti-15 material was around 6 nm for number-weighted, 8 nm for surface-weighted, and 9 nm for volume-weighted analyses. These finding clearly indicate that the postsynthesis NH_4NO_3 treatment of the Ti-SBA-15 support had a significant beneficial effect for obtaining smaller, more uniform gold nanoparticles inside the SBA-15 channels.

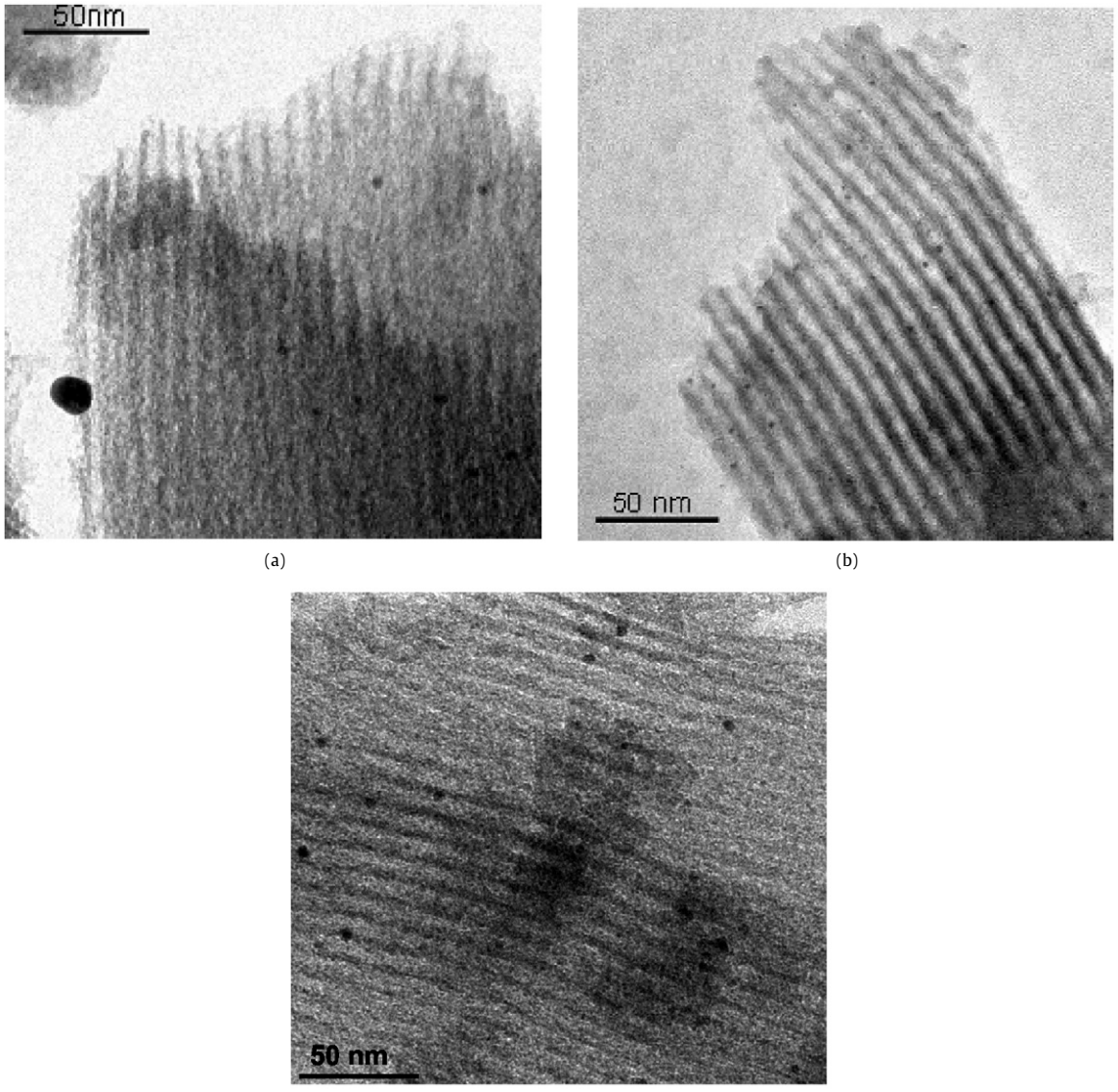

(a) (b)

(c)

Fig. 13. TEM micrographs of: (a) Au-Ti-G, (b) Au/Ti-N-30h, and (c) AuN–Ti-15h.

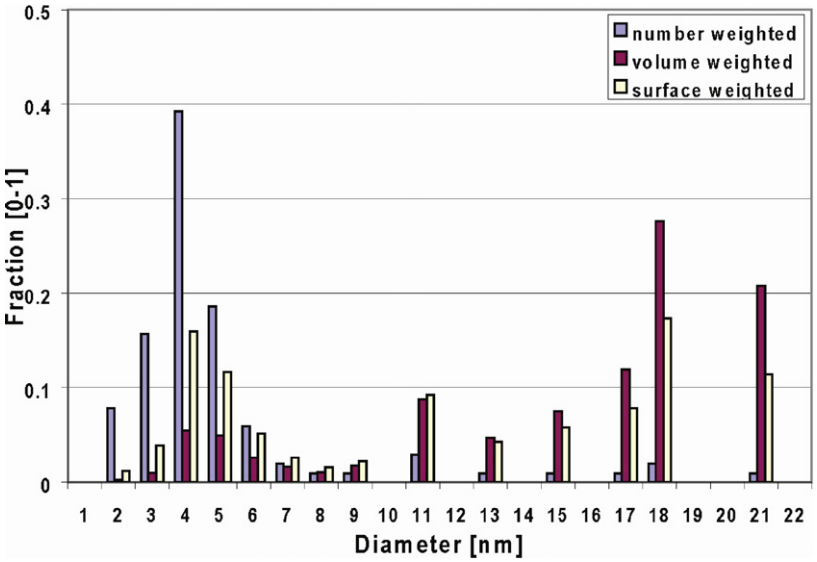

(a)

Fig. 14. Number, surface and volume weighted particle size distributions of: (a) Au-Ti-G, (b) Au/Ti-N-30h, and (c) AuN–Ti-15h.

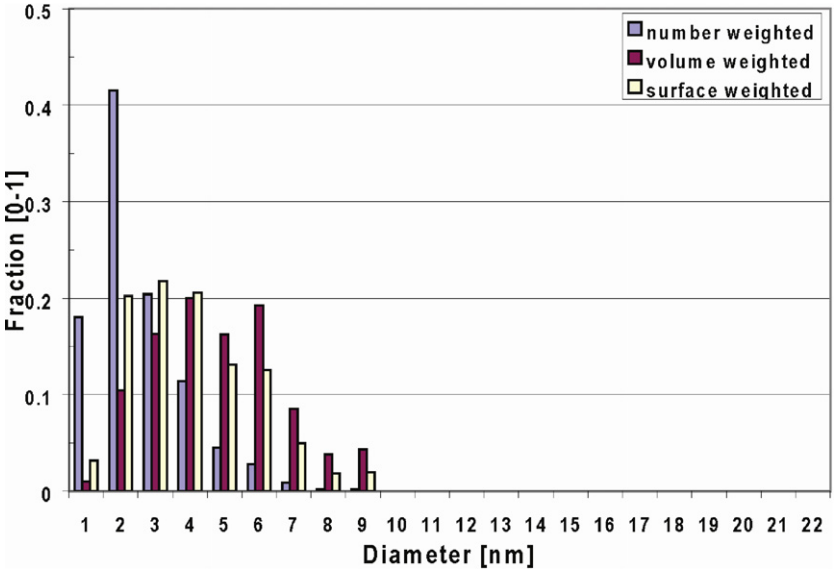

(b)

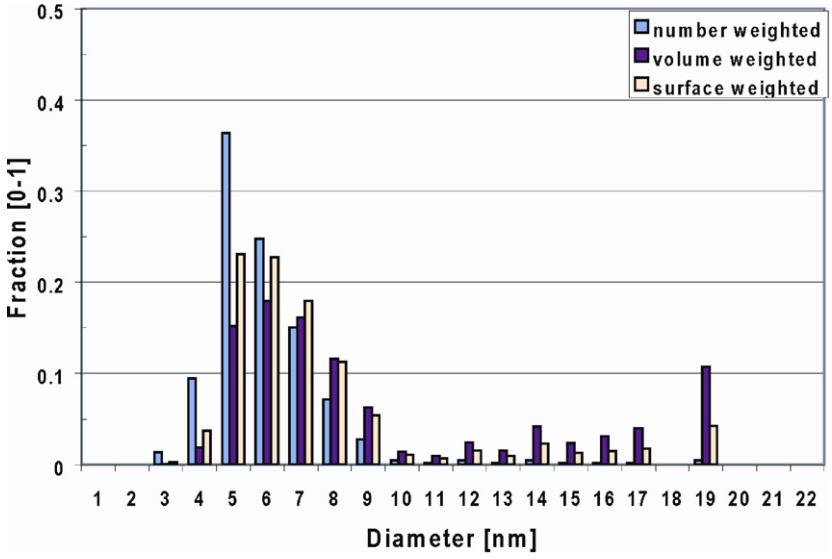

(c)

Fig. 14. (*continued*)

4. Discussion

4.1. Proposed Au deposition mechanism in NH_4NO_3-pretreated Ti-SBA-15

A high intake of gold on a support for TiO_2 requires a high number of available hydroxyl groups as adsorption centers for the gold species [42]. As shown by our NMR findings, pretreatment with NH_4NO_3 significantly increased in the number of hydroxyl groups (Scheme 1). According to the ICP-AES measurements, Au was completely deposited in the NH_4NO_3-pretreated Ti-SBA-15 support. In contrast, in the non-pretreated support, the amount of Au deposited was only 10% of the available gold precursor in the solution. The actual deposition mechanism should be similar to that proposed by Moreau et al. [43], who investigated Au deposition on TiO_2 by studying the effect of pH in the deposition-precipitation process and the species formed at different pH values. When the Ti-SBA-15 support was immersed in the $HAuCl_4$ solution, the pH was 2.6. The pH increased continuously up to a value of 9 through the addition of Na_2CO_3 to obtain the deposited $Au(OH)_3$. In this pH range, the Si–OH groups were gradually transformed into negatively charged $Si–O^-$, but in the 4.5–6 range, the Ti–OH groups were protonated as $Ti–OH_2^+$ [44]. In this pH range, the gold species in solutions were mainly anions $[AuCl_x(OH)_{4-x}]^-$ ($x = 1$–4). This negatively charged species could then be adsorbed on the protonated $Ti–OH_2^+$ groups according to Scheme 2. The electrostatic interaction will be stabilized by the formation of an adsorbed hydroxochloro complex of Au (Scheme 2). This complex will act as a nucleation center for the formation of the $Au(OH)_3$ species [45]. The formation of an Au–amine complex next to the Ti sites was proposed by Delgass et al. [14] to explain the increased Au deposition on a TS-1 support pretreated with 1 M NH_4NO_3. No experimental evidence for this complex was given, but comparing the water-pretreated Ti-H-30h support with the NH_4NO_3 pretreated Ti-N-n supports shows greater gold adsorption on the latter. These findings that along with generating a greater density of hydroxyl groups on the Ti-SBA-15 support, amine species also played a role in the homogeneous deposition of Au. Therefore, we may assume that the presence of amine species in the structure of the Ti-SBA-15 supports enhanced the homogeneous dispersion of gold in to the support. Amine species may be concentrated near to the Lewis acidic Ti sites after postsynthesis

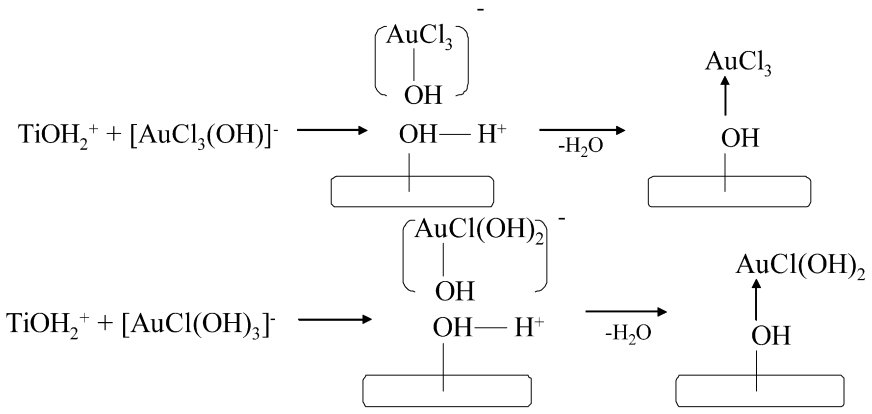

Scheme 2. Mechanism of $HAuCl_4$ deposition on NH_4NO_3 pretreated Ti-SBA-15 at pH <6.

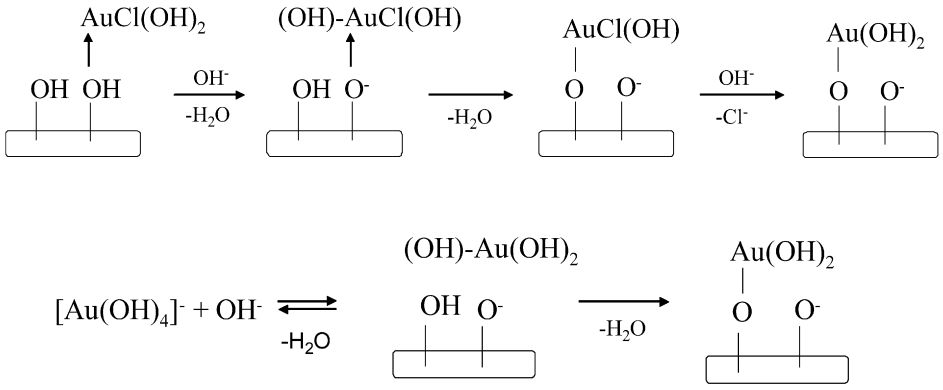

Scheme 3. Mechanism of $HAuCl_4$ deposition on NH_4NO_3 pretreated Ti-SBA-15 at pH >6.

NH_4NO_3 treatment of the Ti-SBA-15 support, causing a more homogeneous deposition of gold nanoparticles in the proximity of Ti sites. This was proven by the results obtained for the AuN/Ti-30h sample when Au was deposited on a NH_4NO_3-treated SBA-15 and Ti was then added. In this latter case, gold was not homogeneously dispersed, because there was no Ti on the support that could concentrate the amine species and facilitate the homogeneous deposition on Ti–OH species. At pH >6, the surface of the Ti-SBA-15 support became negatively charged, due to deprotonation of most of the hydroxyl groups. In solution, the predominant gold species were $AuCl(OH)_3^-$ and $Au(OH)_4^-$. At this pH, the already coordinated $AuCl(OH)_2$ species will react with some possible free OH groups, resulting in the formation of an –O–AuCl(OH) complex (Scheme 3). The $AuCl(OH)_3^-$ and $Au(OH)_4^-$ also can react with the remaining free OH groups on the surface to produce the –O–Au bonds (Scheme 3). Further increases in the pH can transform these species into $Au(OH)_3$. Previous studies of the deposition of gold on TiO_2 have shown decreased Au intake at pH 9. The presence of free hydroxyl groups and amine species on the surface of the Ti-SBA-15 will lead to enhanced adsorption of the gold species starting at a low pH value when the hydroxyl groups are protonated. This increased absorption will occur through electrostatic interaction with anionic gold species, creating a good, uniform absorption of gold from the solution. When the pH is increased from 6 to 9, all of these species will be stabilized by chemical interaction with the support (Scheme 3).

The enhanced activity of Au/Ti-N-n catalyst for the propene epoxidation reaction compared with that of the Au-Ti-G catalyst can be associated with the differences in size and dispersion of the deposited Au nanoparticles in the SBA-15 pore structure. As determined from detailed TEM measurements, the Au particles in the Au/Ti-N-30h catalyst had a number-weighted mean diameter of 2–3 nm, much smaller than that of the Au-G catalyst. Moreover, the differences in volume-weighted mean diameter, from 5 nm (Au/Ti-N-30h) to 15 nm (Au-G), clearly suggest that apart from the low loading of Au present in Au/Ti-G catalyst, a large percentage of the Au atoms were catalytically inactive because they were inaccessible due to the large Au nanoparticles. It is noteworthy that changes in the Au dispersion/particle size between these types of catalysts were related to the different pretreatments of the support with NH_4NO_3. As demonstrated earlier, NH_4NO_3 pretreatment led to better gold adsorption and dispersion due to the increasing number of available adsorption sites at the Ti-SBA-15 surface. Examining the catalytic data in Table 1 for the Au/Ti-N-n (n 6–30 h) pretreated with NH_4NO_3 for different times reveals the greatest PO yield in the sample pretreated for 30 h (Au/Ti-N-30h). Because all of these samples contained the same amount of gold, the difference in activity can be attributed to better dispersion of the gold particles on the support due to the increased number of adsorption sites. UV–vis–NIR DRS spectra of the Ti-SBA-15 supports found titanium also as extra-framework octahedral species. This type of titanium species, known to be responsible for side reactions in propene epoxidation, can be partially removed during NH_4NO_3 pretreatment. Increasing the pretreatment time will then further decrease the amount of these extra-framework Ti species, resulting in increased PO yield.

5. Conclusion

The pretreatment of Ti-SBA-15 support material with NH_4NO_3 before gold immobilization was found to enhance both the gold loading and dispersion. The resulting catalyst materials have enhanced activity in the direct epoxidation of propene with H_2 and O_2 compared with untreated Au-Ti-SBA-15 materials. The main ef-

fect of the NH_4NO_3 pretreatment was related to an increased number of gold adsorption sites at the Ti-SBA-15 surface. This can be explained by the cooperative effect between an increasing number of hydroxyl groups formed by a partial hydrolysis of the ≡Si–O–Si≡ or ≡Ti–O–Si≡ bonds in the Ti-SBA-15 support material and the concentration of amine species in the proximity of Ti sites.

Acknowledgments

Financial support was provided by STW/NWO-VIDI (to T.A.N.), NWO-VICI (to B.M.W.), and NRSC-C (to B.M.W.). The authors thank C. van de Spek for the TEM measurements and A. Mens for the N_2-sorption measurement.

References

[1] T.A. Nijhuis, T. Visser, B.M. Weckhuysen, Angew. Chem. Int. Ed. 44 (2005) 1115; T.A. Nijhuis, T. Visser, B.M. Weckhuysen, J. Phys. Chem. 109 (2005) 19309; T.A. Nijhuis, B.M. Weckhuysen, Chem. Commun. (2005) 6002.
[2] T.A. Nijhuis, B.M. Weckhuysen, Catal. Today 117 (2006) 84.
[3] B. Chowdhury, J.J. Bravo-Suárez, N. Mimura, J. Lu, K.K. Bando, S. Tsubota, M. Haruta, J. Phys. Chem. C 110 (2006) 22995.
[4] T.A. Nijhuis, M. Makkee, J.A. Moulijn, B.M. Weckhuysen, Ind. Eng. Chem. Res. 45 (2006) 3447.
[5] K. Weissermel, H.J. Arpe, in: Industrial Organic Chemistry, second ed., VCH, New York, 1993, p. 141, 264.
[6] T. Hayashi, K. Tanaka, M. Haruta, J. Catal. 178 (1998) 566.
[7] A. Zwijnenburg, M. Makkee, J.A. Moulijn, Appl. Catal. A Gen. 270 (2004) 49.
[8] B. Chowdhury, J.J. Bravo-Suárez, M. Daté, S. Tsubota, M. Haruta, Angew. Chem. Int. Ed. 45 (2006) 412.
[9] M. Haruta, M. Date, Appl. Catal. A Gen. 222 (2001) 427.
[10] A.K. Sinha, S. Seelan, S. Tsubota, M. Haruta, Top. Catal. 29 (2004) 95.
[11] B. Taylor, J. Lauterbach, W.N. Delgass, Appl. Catal. A Gen. 291 (2005) 188.
[12] A.K. Sinha, S. Seelan, T. Akita, S. Tsubota, M. Haruta, Appl. Catal. A Gen. 240 (2003) 243.
[13] A.K. Sinha, S. Seelan, T. Akita, S. Tsubota, M. Haruta, Catal. Lett. 85 (2003) 3.
[14] L. Cumaranatunge, W.N. Delgass, J. Catal. 232 (2005) 38.
[15] A. Corma, M.T. Navarro, J. Pérez-Pariente, J. Chem. Soc. Chem. Commun. (1994) 147.
[16] S. Gontier, A. Tuel, J. Catal. 157 (1995) 124.
[17] T.A. Nijhuis, B.J. Huizinga, M. Makkee, J.A. Moulijn, Ind. Eng. Chem. Res. 38 (1999) 884.
[18] E.E. Stangland, K.B. Stavens, R.P. Andres, W.N. Delgass, J. Catal. 191 (2000) 332.
[19] B.S. Uphade, M. Okumura, S. Tsubota, M. Haruta, Appl. Catal. A Gen. 190 (2000) 43.
[20] B.S. Uphade, Y. Yamada, T. Akita, T. Nakamura, M. Haruta, Appl. Catal. A Gen. 215 (2001) 137.
[21] B.S. Uphade, T. Akita, T. Nakamura, M. Haruta, J. Catal. 209 (2002) 331.
[22] E. Sacaliuc, A.M. Beale, B.M. Weckhuysen, T.A. Nijhuis, J. Catal. 248 (2007) 235.
[23] D. Trong On, D. Desplamtier-Giscard, C. Danumah, S. Kaliaguine, Appl. Catal. A Gen. 222 (2001) 299.
[24] C. Qi, T. Akita, M. Okumura, K. Kuraoka, M. Maruta, Appl. Catal. A Gen. 253 (2003) 75.
[25] M. Haruta, Catal. Today 36 (1997) 153.
[26] N. Yap, R.P. Andres, W.N. Delgass, J. Catal. 226 (2004) 156.
[27] D. Zhao, J. Feng, Q. Huo, N. Melosh, B.F. Chmelka, G.D. Stucky, J. Am. Chem. Soc. 120 (1998) 26024.
[28] X. Gao, S.R. Bare, J.L.G. Fierro, M.A. Banares, I.E. Wachs, J. Phys. Chem. B 102 (1998) 5653.
[29] A.H. Janssen, C.-M. Yang, Y. Wang, F. Schüth, A.J. Koster, K.P. de Jong, J. Phys. Chem. B 107 (2003) 10552.
[30] H. Friedrich, J.R.A. Sietsma, P.E. de Jongh, A.J. Verkleij, K.P. de Jong, J. Am. Chem. Soc. 129 (2007) 33.
[31] U. Ziese, K.P. de Jong, Appl. Catal. A Gen. 260 (2004) 71.
[32] K.S.W. Sing, D.H. Everett, R.A.W. Haul, L. Moscow, R.A. Pierotti, J. Rouquerol, T. Siemieniewska, Pure Appl. Chem. 57 (1985) 603.
[33] P. Van Der Voort, P.I. Ravikovitch, K.P. De Jong, M. Benjelloun, E.A. Van Bavel, H. Janssen, A.V. Neimark, B.M. Weckhuysen, E.F. Vansant, J. Phys. Chem. B 106 (2002) 5873; P. Van Der Voort, P.I. Ravikovitch, K.P. de Jong, A.V. Neimark, A.H. Janssen, M. Benjelloun, E. Van Bavel, P. Cool, B.M. Weckhuysen, E.F. Vansant, Chem. Commun. (2002) 1010.
[34] G. Ricchiardi, A. Damin, S. Bordiga, C. Lamberti, G. Spano, F. Rivetti, A. Zecchina, J. Am. Chem. Soc. 121 (2001) 11409.
[35] S. Bordiga, S. Coluccia, C. Lamberti, L. Marchese, A. Zecchina, F. Boscherini, F. Buffa, F. Genoni, G. Leofanti, G. Petrini, G. Vlaic, J. Phys. Chem. 98 (1994) 4125.
[36] D. Trong On, S. Nguyen, V. Hulea, E. Dumitriu, S. Kaliaguine, Microporous Mesoporous Mater. 57 (2003) 169.
[37] M.C. Daniel, D. Astruc, Chem. Rev. 104 (2004) 239.
[38] C.A. Fyfe, G.C. Gobbi, G.J. Kennedy, J. Phys. Chem. 89 (1985) 277.
[39] Z. Luan, H. He, W. Zhou, J. Klinowski, J. Chem. Soc., Faraday Trans. 94 (1998) 979.
[40] L. Marchese, E. Gianotti, V. Dellarocca, T. Maschmeyer, F. Rey, S. Coluccia, J.M. Thomas, Phys. Chem. Chem. Phys. 1 (1999) 585.
[41] R.J. Matyi, L.H. Schwartz, J.B. Butt, Catal. Rev. Sci. Eng. 29 (1987) 41.
[42] R. Zanella, L. Delannoy, C. Louis, Appl. Catal. A Gen. 291 (2005) 62.
[43] F. Moreau, G.C. Bond, A.O. Taylor, J. Catal. 231 (2005) 105.
[44] P. Inego, G. Aprile, M.D. Serio, D. Gazzoli, E. Sactacesaria, Appl. Catal. A Gen. 178 (1999) 97.
[45] G.C. Bond, C. Louis, D.T. Thompson, in: G.J. Hutchings (Ed.), Catalysis by Gold, in: Catal. Sci. Ser., vol. 6, Imperial College Press, London, 2006.